# Structural and optical study of Zn-doped $As_2Se_3$ thin films: Evidence for photoinduced formation of ZnSe nanocrystallites

Cite as: AIP Advances 9, 065212 (2019); doi: 10.1063/1.5086974
Submitted: 26 December 2018 • Accepted: 8 March 2019 •
Published Online: 18 June 2019



Yu. M. Azhniuk,[1,2,a)] D. Solonenko,[3] E. Sheremet,[3,4] V. M. Dzhagan,[3,5] V. Yu. Loya,[1] I. V. Grytsyshche,[1] S. Schulze,[6] M. Hietschold,[6] A. V. Gomonnai,[1,2] and D. R. T. Zahn[3]

## AFFILIATIONS

[1]Institute of Electron Physics, Ukr. Nat. Acad. Sci., 21 Universytetska Str., 88017 Uzhhorod, Ukraine
[2]Uzhhorod National University, 46 Pidhirna Str, 88000 Uzhhorod, Ukraine
[3]Semiconductor Physics, Chemnitz University of Technology, D-09107 Chemnitz, Germany
[4]Tomsk Polytechnic University, 30 Lenina Ave., 634034 Tomsk, Russia
[5]V. Lashkaryov Institute of Semiconductor Physics, Ukr. Nat. Acad. Sci., 45 Prospect Nauky, 03028 Kyiv, Ukraine
[6]Solid Surface Analysis, Chemnitz University of Technology, D-09107 Chemnitz, Germany

[a)]**E-mail:** yu.azhniuk@gmail.com

## ABSTRACT

Amorphous Zn-doped $As_2Se_3$ films with a nominal zinc content $x$ up to 10 at.% were prepared by thermal evaporation. Their structure is characterized by atomic force microscopy (AFM), scanning electron microscopy (SEM), energy-dispersive X-ray spectroscopy (EDX), X-ray photoemission spectroscopy (XPS), and Raman spectroscopy. The AFM data show a considerable increase of the film surface roughness for films with $x > 5$ at.%. A strong gradient of the Zn content decreasing into the film depth is confirmed by the EDX and XPS data. Heavily Zn-doped (above 7 at.%) $As_2Se_3$ films reveal photostructural changes in the course of the Raman measurements. New Raman features are attributed to TO and LO vibrations of ZnSe nanocrystallites formed in the film under laser illumination. Depending on the laser wavelength and power density, the ZnSe nanocrystallites can experience tensile strain in the film due to a non-thermal photoplastic effect in the $As_2Se_3$ film resulting in a partial removal of the material from the laser spot. The tensile strain value, estimated from the TO and LO phonon frequency shift, is shown to reach up to 2.9 GPa.



## I. INTRODUCTION

Amorphous arsenic selenide $As_2Se_3$ is a well-known semiconductor material which attracts the interest of researchers due to its numerous possible applications. Being exposed to light of appropriate energy and intensity, non-crystalline arsenic chalcogenides often undergo changes of their electronic and atomic structure, composition, phase, physical and chemical properties generally known as photoinduced effects [Refs. 1–5 and references therein]. Such changes have led to extensive applications of amorphous chalcogenides, the most well known of them being related to optical data storage [Refs. 4, 6 and references therein]. The wide transparency range in the infrared spectral region makes amorphous $As_2Se_3$ a suitable material for microstructured optical fibres,[7,8] holographic gratings,[7,9] and planar waveguides.[7,10] Photoinduced effects in amorphous chalcogenides are used in xerography, photovoltaic and photoconductive elements, laser printers, light-sensitive camera tubes, high-speed optical switches, and X-ray radiography [Refs. 1–4, 11 and references therein].

$As_2Se_3$ films and bulk glasses are known to undergo photostructural changes under illumination which can be reversible or irreversible. The photostructural changes can be driven by thermal or non-thermal mechanisms and strongly depend on the illumination conditions as well as the film preparation details and

thermal history.[2–4] Along with other techniques,[2–4,12–14] Raman spectroscopy was often employed to investigate the photoinduced structural changes in amorphous arsenic chalcogenides.[4,15–18]

Contrary to the extensively investigated amorphous As–Se systems with different As and Se content ratio, studies of doped amorphous $As_2Se_3$, except for the Ge–As–Se systems, are rather rare. Nevertheless, it was shown that optical and electrical properties of amorphous $As_2Se_3$ can be noticeably modified by doping.[7,19,20] Moreover, in an amorphous chalcogenide with a high dopant content one can also expect photoinduced phase separation when part of the material crystallizes in a surrounding amorphous matrix similar to more complex $As_2Se_3$-based[21] or $As_2S_3$-based[22,23] materials. Recently, reversible athermal crystallization under above-bandgap illumination was observed by time-resolved Raman spectroscopy for a related amorphous Ga–Ge–Sb–S chalcogenide[24] showing the way to prepare glass-ceramic composites with varying glass-to-crystal fraction. Non-thermal photostructural processes have the potential for a bond-specific engineering of glassy structures for photonic applications with a spatial resolution that is not achievable by thermal annealing.[24]

Here we report on a study of Zn-doped $As_2Se_3$ thin films grown by a thermal evaporation technique using atomic force microscopy (AFM), scanning electron microscopy (SEM) combined with energy-dispersive X-ray spectroscopy (EDX), X-ray photoelectron spectroscopy (XPS) as well as micro-Raman spectroscopy.

## II. EXPERIMENTAL

Two batches of Zn-doped $As_2Se_3$ films on silicon and silicate glass substrates with Zn content $x$ ranging from 0.7 to 10 at.% were prepared. For $As_2Se_3$ preparation the initial elemental components were additionally refined to a purity of 99.9999 %. For one batch, the mixture of $As_2Se_3$ and Zn in the desired proportion was loaded in a tantalum Knudsen cell, the evaporation was carried out at 770–830 °C at a rate of 6 nm/s. For the second batch, Zn-doped $As_2Se_3$ glasses were synthesized from extra refined elemental components at 420–460 °C in quartz ampoules evacuated to $10^{-4}$ Torr. Then the powdered blend was continuously fed in the form of fine grains into a tantalum evaporator heated to 770–830 °C. This so-called flash evaporation technique[25] enables the composition of the vapor produced to be closely approximated to that of the starting material. The evaporation rate was approximately 8 nm/s. In both cases the evaporation was performed at $10^{-5}$ Torr, the substrates were kept at room temperature. The thickness of the films produced was within the range of 1.7–2.1 μm.

AFM measurements were performed using an Agilent AFM 5420 with an additional piezoelectric scanner from nPoint Inc. using commercial silicon NGS-01A tips (curvature radius 10 nm) in intermittent mode. Several AFM scans were performed for each sample to ensure the uniformity of the parameters obtained over the sample surface.

SEM and EDX measurements were carried out using a NovaNanoSEM microscope from FEI operating at different electron energies (from 5 to 30 keV) to vary the probing depth.

XPS measurements were performed using an ESCALAB 250Xi XPS Microprobe (Thermo Scientific) equipped with a monochromatized Al Kα X-ray source ($h\nu$ = 1486.6 eV). The survey and high-resolution spectra were acquired at bandpass energies of 200 eV and 20 eV, respectively. The surface charging from photoelectron emission was neutralized using a low-energy (<10 eV) electron flood gun. Argon ion sputtering was employed to clean the film surface and XPS spectra were sequentially recorded from the sputtered area after each 30 s sputtering session in order to check their variation with the film depth.

Spectroscopic ellipsometry measurements were carried out for the initial film and for the sputtered area using a J.A.Woolam M-2000 ellipsometer. The analysis of the ellipsometry data was performed using CompleteEASE software which enabled us, in particular, to determine the thicknesses of the film before and after sputtering and thus to estimate the rate of removal of the film material from its surface. To model the layer of arsenic selenide film, a Cauchy model was used in the energy range below its bandgap.

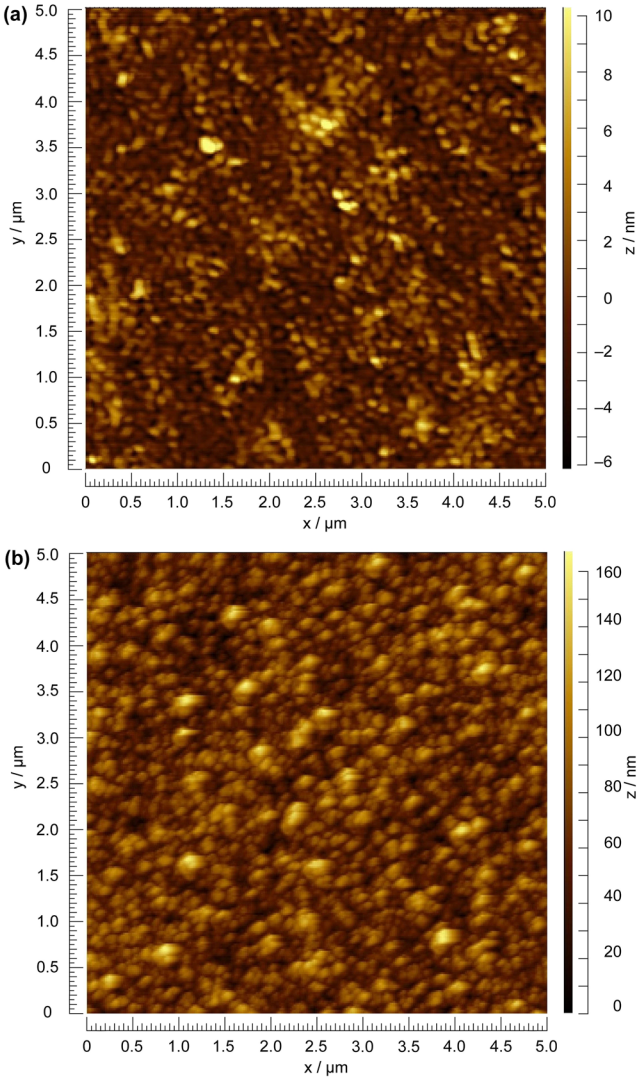


**FIG. 1**. AFM surface topography of Zn-doped $As_2Se_3$ films: (a) nominal zinc content 5 at.%, surface roughness $R_a$ = 1.7 nm, (b) nominal zinc content 10 at.%, surface roughness $R_a$ = 17.4 nm.

Micro-Raman studies were carried out at room temperature using a $Kr^+$ laser (568.2 nm, 647.1 nm, and 676.4 nm lines) and a Dilor XY 800 spectrometer equipped with a CCD camera. The spectral resolution was better than 2.5 $cm^{-1}$. The laser power was reduced down to values ensuring Raman spectra stability and afterwards gradually increased in order to observe the dynamics of the photoinduced changes in the Raman spectra during the measurements. For each measurement a new spot was chosen on the film surface in order to eliminate the photoinduced changes related to previous measurements.

## III. RESULTS

AFM images of pure and low-Zn (nominal content $x$ up to 5 at.%) $As_2Se_3$ films exhibit a rather uniform pattern with relatively small surface roughness $R_a$ ranging from 1.1 to 3.3 nm (Fig. 1a). Meanwhile, the $As_2Se_3$ films with higher nominal content of zinc are much rougher. Their roughness $R_a$ ranges from 17 to 44 nm (See Fig. 1b). Note that no significant difference in the surface roughness was observed for films of similar composition from the two different batches.

SEM studies combined with EDX measurements carried out at different electron energies (from 5 to 30 keV) which provided different probing depths, enabled us to check the chemical composition of the films obtained and its variation over the film thickness. Figure 2 shows the corresponding spectra for the sample with the nominal zinc content $x$ of 10 at.% as well as the element content calculated from the spectra.

As follows from the EDX data, the zinc content in the film corresponds to the nominal value of 10 at.% only for the lowest exciting electron energy applied (5 keV). Meanwhile, for higher electron energy values the Zn content strongly decreases down to 2 at.% for energies of 20–30 keV. The EDX measurements performed for other samples of the Zn-doped $As_2Se_3$ films reveal a similar sharp decrease of the Zn content from the surface into the film depth. A clear qualitative agreement is observed between the nominal Zn concentration in the film and the value of zinc content in the surface layer of the film evaluated from the EDX data for the minimal electron energy (5 keV). Hence, it seemed reasonable for us to refer to the film samples by quoting the nominal Zn content $x$, even though actually the Zn content is variable, decreasing from the film surface into its depth. Note that the EDX spectra-based element concentration data for the films of the same nominal composition obtained on different (silicon and silicate glass) substrates showed a remarkable coincidence and good reproducibility. Even though, due to the limitations of the EDX technique, we could not build explicit depth profiles of the Zn content in the films under study, the data obtained give a clear qualitative evidence of the zinc concentration gradient, decreasing with the film depth.

The survey XPS spectra (not shown) of the sputtered films revealed only the core-level and Auger peaks of As, Se, and Zn. Representative high-resolution XPS spectra are shown in Fig. 3. The binding energies (BEs) of Zn 2$p$ coincide well with values expected for semiconductor compounds.[26] The lineshape of Se 3$d$ spectrum requires two-component fitting, with Se $3d_{5/2}$ BEs of 54.5 and 55.3 eV, respectively (Fig. 3b). As follows from Ref. 27, they

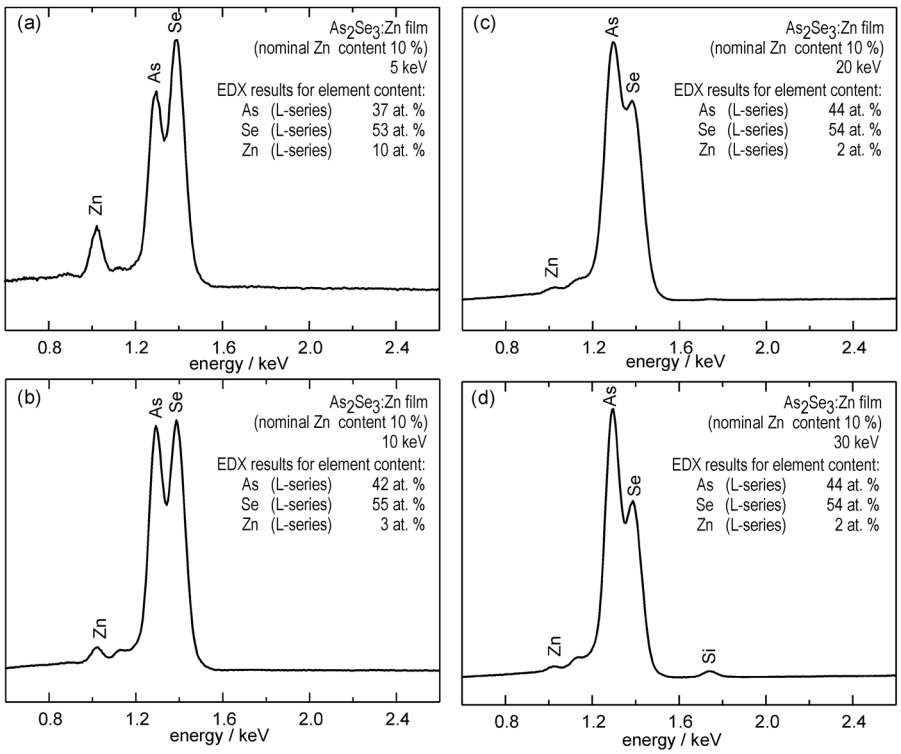


**FIG. 2.** EDX spectra of a Zn-doped $As_2Se_3$ film with the nominal zinc content of 10 at.% on a silicon substrate at different exciting electron energies: (a) 5 keV, (b) 10 keV, (c) 20 keV, and (d) 30 keV. The composition of the film calculated from the spectra is obtained after the subtraction of the silicon content determined by the signal from the substrate.

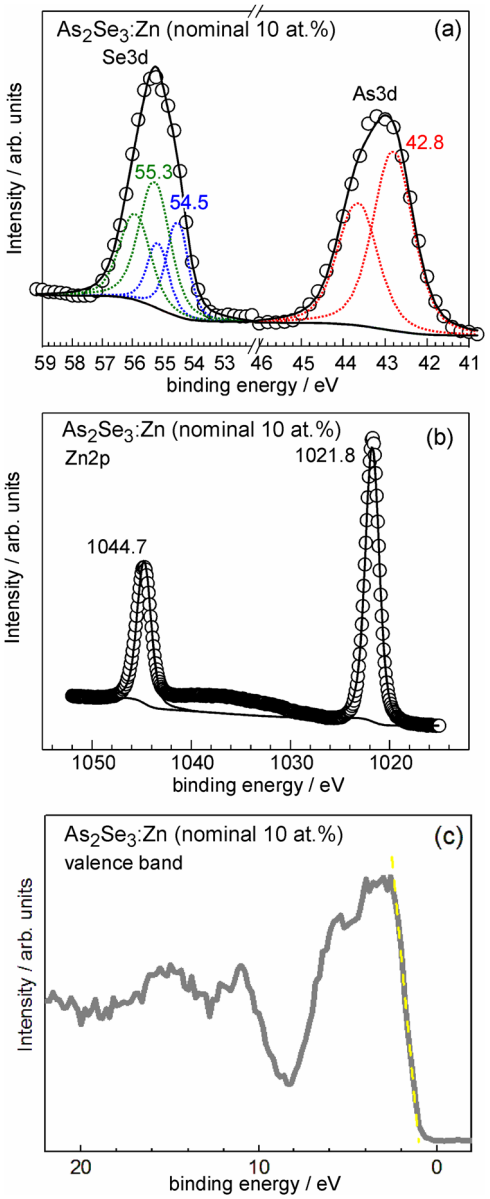


**FIG. 3**. Representative high-resolution XPS spectra of As3*d* and Se3*d* (a) and Zn2*p* (b) orbitals as well as the valence band spectrum (c) for the $As_2Se_3$:Zn film with nominal Zn content of 10 at. %.

can be attributed to two different configurations of Se, presumably Se–AsAs and Se–SeAs. However, in our case, as follows from the EDX studies, the concentration of zinc atoms on the film surface is quite high and one cannot preclude the possibility for the existence of Zn–Se bonds. Moreover, as the BEs for Se 3*d* in $As_2Se_3$ and ZnSe are quite close and definitely belong to the relevant range (55.3 and 54.7 eV, respectively[28]), the two Se $3d_{5/2}$ peaks in question can be alternatively attributed to Se–As and Se–Zn bonds. Both explanations seem to be reasonable and an exact assignment of the two peaks under consideration would require a targeted study. The As 3*d* spectrum can be well fitted with a single component at 42.8 eV (As $3d_{5/2}$), though its relative large FWHM (1.5 eV) can be related to a second component with a close BE. The Se and As spectra are generally in agreement with the literature data for stoichiometric and nearly stoichiometric $As_2Se_3$.[14,27–32] However, even though numerous studies reported systematic and consistent variation of the As 3*d* and Se 3*d* binding energies with the atomic configuration (and the corresponding As:Se content ratio), the difference in the binding energies of Se 3*d* for different studies is up to 0.7 eV (*e.g.* Refs. 14, 26, and 32 versus Refs. 27 and 28), while for As *3d* very close values are obtained. In Refs. 29 and 30 the BEs of Se in amorphous $As_2Se_3$ coincide with those in Refs. 14 and 26, but for As *3d* the BE is lower by about 0.7 eV than obtained in Refs. 14, 26–28. As the possible contribution of the Zn–Se bond lies within the BE range of the two discussed As–Se bonding configurations, it is not possible to resolve the effect of the former on the FWHM of the Se 3*d* band, especially within the range of relatively small variation of the Zn content.

The lineshape of the valence band region (Fig. 3c) is in good agreement with previous reports on $As_2Se_3$,[14,27] including the 1 eV shift of the valence band edge with respect to the Fermi energy (0 eV in Fig. 3c). A more detailed analysis of the XPS data will be reported elsewhere.

XPS spectra sequentially measured from an $Ar^+$ ion sputtered area enabled us to build the profiles of arsenic, selenium and zinc concentrations versus the film depth. The film material removal rate was determined based on the film thickness values inside and outside the sputtered area determined from the ellipsometry data. The relevant data, summarized in Fig. 4, clearly confirm the depth gradient of the Zn concentration, decreasing inwards the film. Both the content of zinc on the film surface and the thickness of the zinc-containing layer qualitatively correlate with the nominal Zn content. It can be seen that for the sample with nominal 10 at. % of Zn the top surface layer of the film exhibits quite a high zinc content nearly corresponding to ZnSe with only a slight additive of arsenic. However, with increasing thickness of the sputtered layer (*i.e.* going deeper inwards the film) a sharp drop of zinc concentration is observed. For probing deeper than 10 nm (for the sample with nominal 7 at. % Zn) and 80 nm (nominal 10 at. % Zn) the chemical composition of the film corresponds to the $As_2Se_3$ formula, showing not more than mere traces of zinc.

Note that for the Zn-doped $As_2Se_3$ films with relatively high Zn concentrations (above 7 at.%) the accuracy of the element content depth profiles based on the XPS data is also affected by the noticeably increased surface roughness of 17 to 44 nm as followed from the AFM data. On the other hand, the increased concentration of Zn in the surface layer of the $As_2Se_3$ films with high Zn content and the increasing number of Zn–Se bonds formed on the surface (which follows from the depth profiles in Fig. 4) can be a reason for the much higher roughness of the high-Zn $As_2Se_3$ films observed in the AFM images (Fig. 1).

The amorphous structure of the films obtained is confirmed by Raman spectroscopy. As it can be seen from Fig. 5, a single broad asymmetric maximum near 225 $cm^{-1}$ with a more pronounced lower-frequency side is observed for all samples in the case that the laser excitation power is low enough not to result in any changes in the spectra within the illumination time. The position and the width

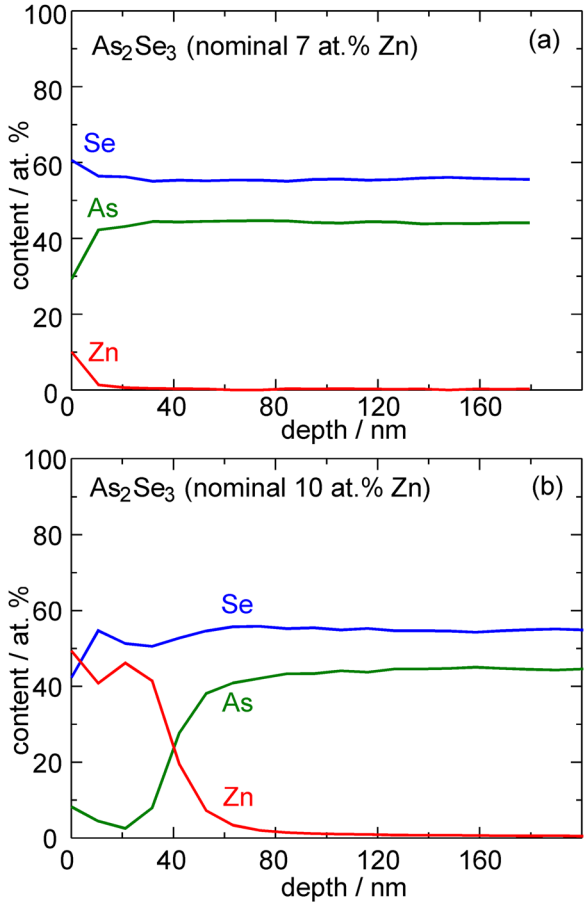


**FIG. 4**. Depth profiles of the Zn content obtained from XPS spectra for a Zn-doped $As_2Se_3$ film with the nominal zinc content of 7 % (a) and 10 % (b).

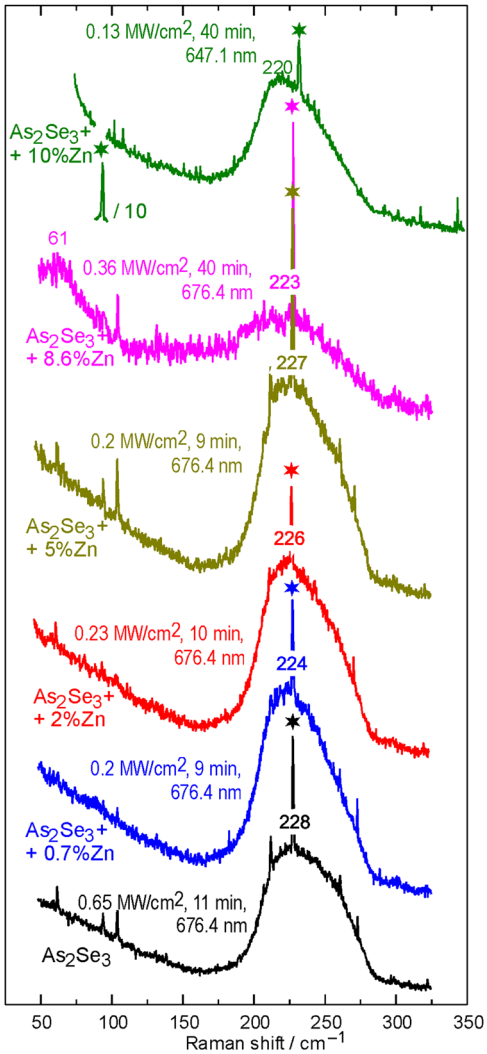


**FIG. 5**. Raman spectra of nominally pure and Zn-doped $As_2Se_3$ films measured at laser beam wavelengths and power densities low enough to provide spectrum stability within the illumination time. The relevant laser beam illumination parameters (power density, time, and wavelength) are shown for each spectrum. The acquisition time was 1 min (except for the topmost curve where due to the small excitation power density the acquisition time was increased to 40 min). Asterisks mark the $Kr^+$ laser plasma lines.

of the maximum are in good agreement with the Raman data known for amorphous $As_2Se_3$.[15,33,34]

Note that for arsenic chalcogenide films, similarly to the bulk materials,[17,35–37] one can observe a photoplastic effect consisting in a light-induced variation of the glass mechanical properties, *i.e.* its softening and a radial mass transfer of the material from the laser spot. This effect did not enable us to vary the excitation laser power density $P_{exc}$ in a very broad range since the power increase resulted in the formation of a pit in the laser spot which led to beam defocusing (reducing thereby the power density) or even (in case of a thin film) a hole burnt in the material. This set the upper limit of the achievable power density which varied depending on the dopant concentration and the excitation wavelength. The lower limit of the power density was set by a reasonable signal-to-noise ratio required to analyze the observed Raman spectrum. Still, even in a relatively narrow power density range we could observe a different behavior of the films depending on the zinc content in them.

For nominally pure and low-Zn (*i. e.* with nominal Zn content below 5 at.%) $As_2Se_3$ films the shape of the Raman spectra does not depend on the illumination time and the laser power density. However, for the films with higher zinc content the Raman spectra are observed to vary with the excitation laser power density and wavelength as well as the illumination time.

For $As_2Se_3$ films doped with 7 at.% Zn at a low 647.1 nm laser power density of 0.2 MW/cm$^2$ (Fig. 6) the spectra recorded immediately after the laser beam onset and after the sample illumination for 15 min are practically identical. Therefore, one may conclude that the amorphous films are structurally stable under such conditions.

However, at a higher power density of 0.4 MW/cm$^2$ (Fig. 7) even the Raman spectrum measured immediately after the illumination onset (within the first minute) reveals a deviation from the

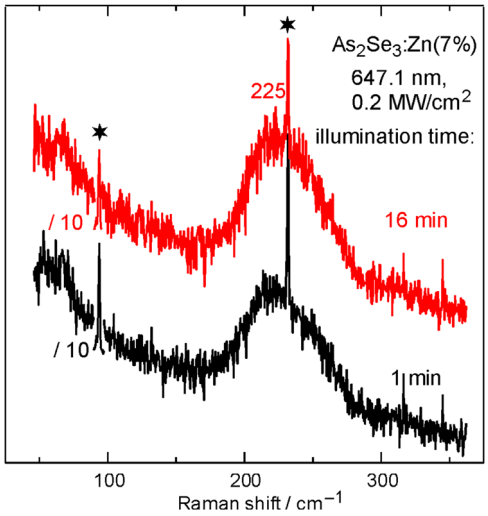


**FIG. 6**. Raman spectra of an $As_2Se_3$:Zn film with the nominal zinc content of 7 at.% measured using a laser wavelength of 647.1 nm and a power density of 0.2 MW/cm$^2$. The acquisition time was 1 min. Asterisks mark the $Kr^+$ laser plasma lines.

spectra observed for the same sample at lower power density (Fig. 6) as well as for the samples with a lower content of Zn in the material at higher $P_{exc}$: the lineshape of the Raman band is more symmetrical with the maximum position shifted slightly to 230 cm$^{-1}$ (the bottom curve in Fig. 7a). In the course of the illumination a second peak at 250 cm$^{-1}$ on the high-frequency side of the Raman band gradually grows. The experimentally observed spectra are well fitted by two Lorentzian contours (a typical example of fitting is shown for the spectrum corresponding to the illumination time of 8 min in Fig. 7a). It is important to notice that the peak positions of both Lorentzians (220–223 and 251–253 cm$^{-1}$) as well as their halfwidths (see Fig. 7b) remain practically unchanged with the illumination time while the intensity of the maximum near 250 cm$^{-1}$ exhibits a constant sublinear growth (Fig. 7b).

In a similar way, for the $As_2Se_3$ film doped with 8.6 at.% Zn, at a rather low 647.1 nm laser power density of 0.4 MW/cm$^2$ the Raman spectrum shown in Fig. 8a remains the same with time indicating that the film structure at such illumination conditions does not change. At a somewhat higher power density (0.6 MW/cm$^2$) even after the first minute of illumination the Raman spectrum is different, revealing two overlapping humps at roughly 200 and 250 cm$^{-1}$. Nevertheless, this spectrum remains stable within a relatively long illumination time of 11 min (Fig. 8b). If the laser power density is further increased (0.8 MW/cm$^2$), the Raman spectrum is changed more noticeably with two clear peaks observed at 196 and 242 cm$^{-1}$ after the first minute of illumination which become somewhat more pronounced and diverged (194 and 244 cm$^{-1}$) within the subsequent 3 min of illumination (Fig. 8c).

If a shorter-wavelength laser line (568.2 nm) is used for the excitation, the behaviour of the $As_2Se_3$:Zn (8.6 at.%) film Raman spectra is almost exactly the same (see Fig. 9), with the only difference that the illumination-induced changes in the spectra are revealed at power density values reduced approximately by half

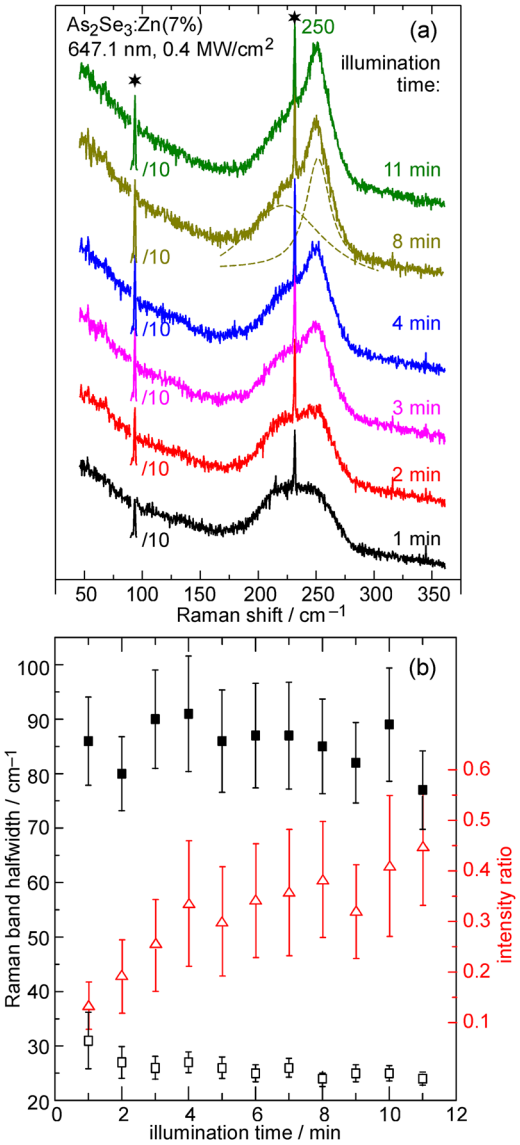


**FIG. 7**. (a): Evolution of the Raman spectra of the Zn-doped (nominal content of 7 at.%) $As_2Se_3$ film measured using a laser wavelength of 647.1 nm and a power density of 0.4 MW/cm$^2$ with the illumination time. The acquisition time was 1 min. Asterisks mark the $Kr^+$ laser plasma lines. An example of fitting is shown for the illumination time of 8 min by dashed curves; (b): time dependences of halfwidths for the broad peak near 222 cm$^{-1}$ (dark squares) and the narrower peak near 250 cm$^{-1}$ (open squares) as well as the ratio of the integrated intensities of the peak near 250 cm$^{-1}$ and the maximum near 222 cm$^{-1}$ (open triangles).

in comparison with $\lambda_{exc}$ = 647.1 nm. This confirms a clear relation of the photoinduced structural changes in the film with the energy of the illuminating light. Note that the energy of the three laser lines used is higher than the $As_2Se_3$ optical band gap (near 1.75 eV).[38] The observed behaviour correlates well with the increasing optical absorption of $As_2Se_3$ glass with the above-bandgap light frequency.[39]

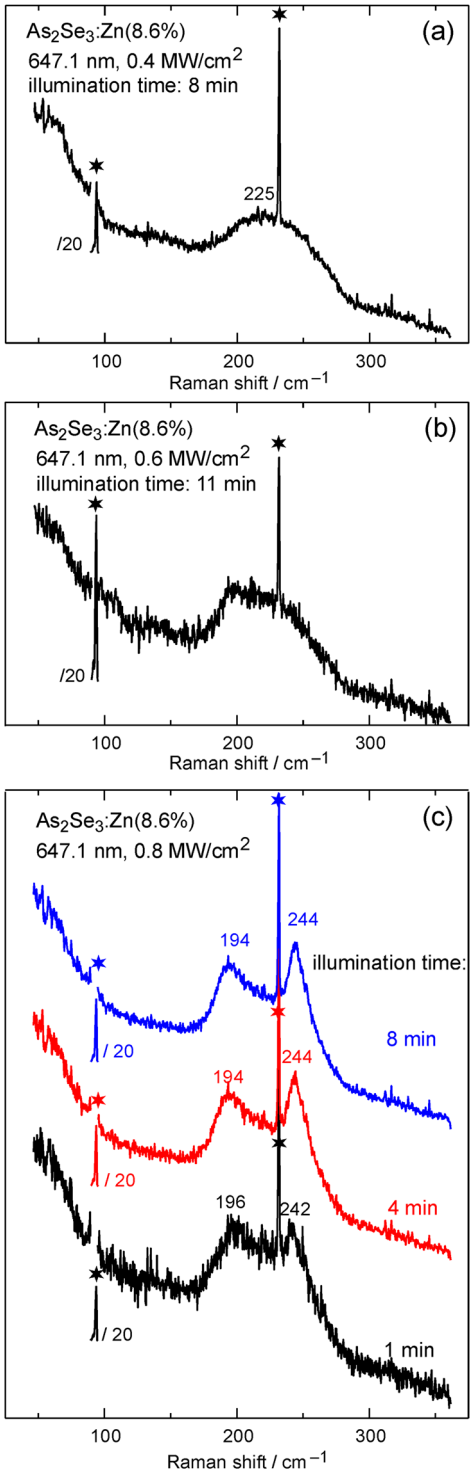


**FIG. 8**. Raman spectra of the Zn-doped ($x$ = 8.6 at.%) $As_2Se_3$ film measured using different 647.1 nm laser power densities: (a) $P_{exc}$ = 0.4 MW/cm$^2$, (b) $P_{exc}$ = 0.6 MW/cm$^2$ – the spectra do not vary with the illumination time; (c) spectra measured at $P_{exc}$ = 0.8 MW/cm$^2$ at the variation of the illumination time. Asterisks mark the $Kr^+$ laser plasma lines.

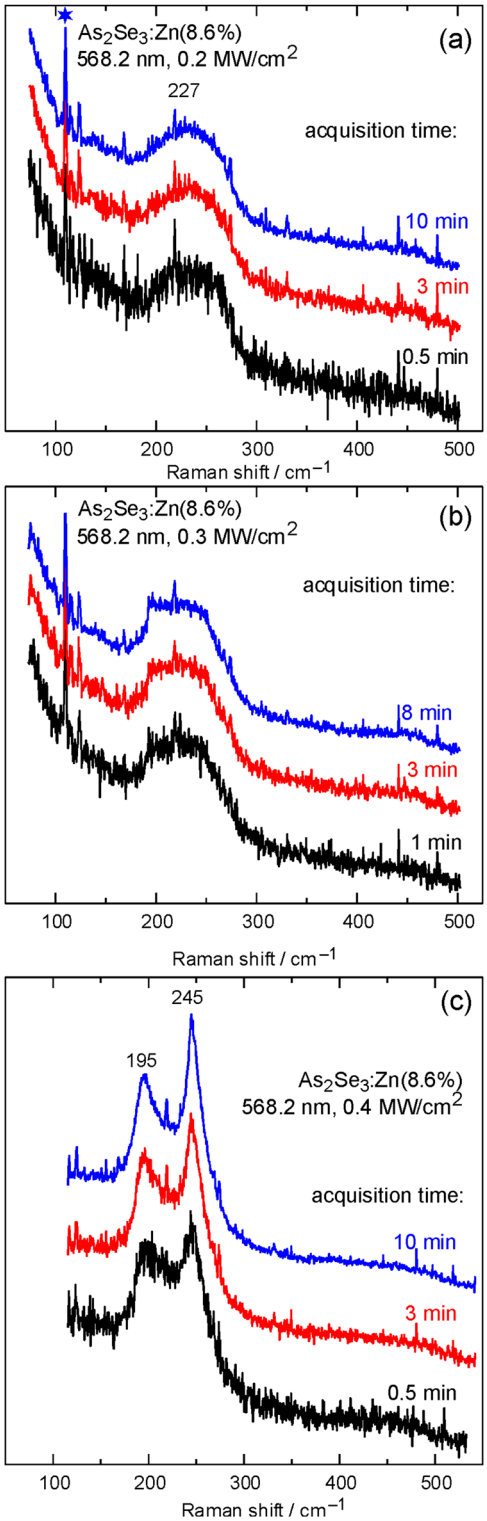


**FIG. 9**. Raman spectra of the Zn-doped ($x$ = 8.6 at.%) $As_2Se_3$ film measured using different 568.2 nm laser power densities at the variation of the illumination time. Asterisks mark the $Kr^+$ laser plasma lines.

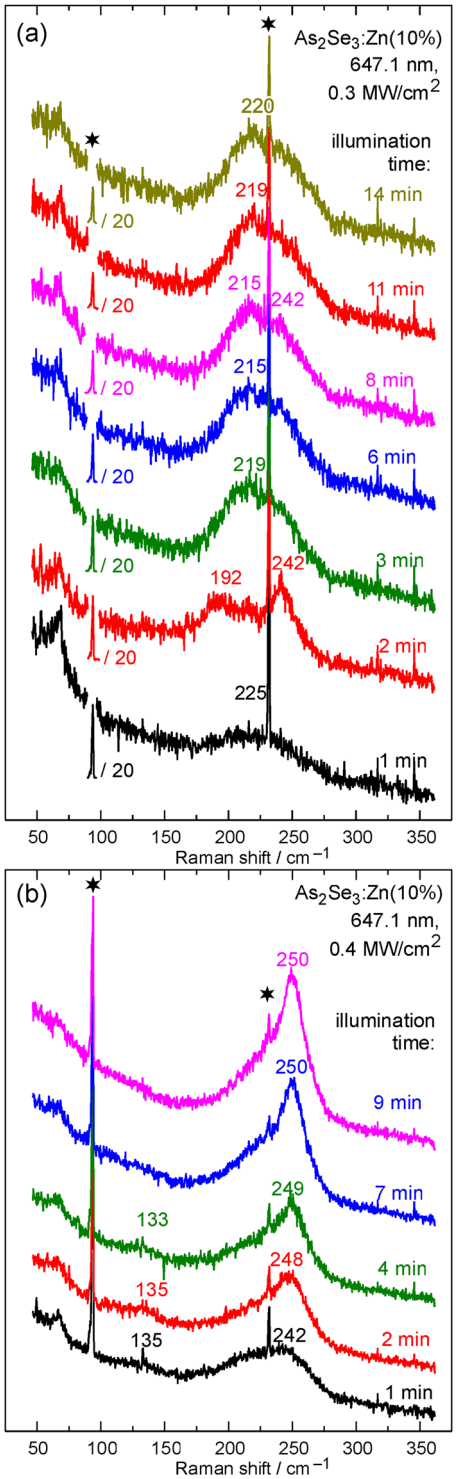


**FIG. 10**. Raman spectra of the Zn-doped ($x$ = 10 at.%) $As_2Se_3$ film measured using a laser wavelength of 647.1 nm at laser power densities of 0.3 MW/cm$^2$ (a) and 0.4 MW/cm$^2$ (b) at the variation of the illumination time. The acquisition time was 1 min. Asterisks mark the $Kr^+$ laser plasma lines.

For the most heavily (10 at.%) zinc-doped $As_2Se_3$ film the Raman spectra measured at a rather low 647.1 nm laser beam power density of 0.3 MW/cm$^2$ (Fig. 10a) reveal a strongly non-monotonous behaviour with the illumination time. While within the first minute of illumination the spectrum remains as typical for amorphous $As_2Se_3$ with the broad maximum at 225 cm$^{-1}$ (bottom curve in Fig. 10a), during the second minute it rapidly changes revealing two clear maxima at 192 and 242 cm$^{-1}$. Rather surprisingly, within the third minute of illumination the spectrum changes back to an "amorphous-like" one with a somewhat lower maximum position (215 cm$^{-1}$), basically retaining this character thereafter, though a shoulder near 242 cm$^{-1}$ can be observed after 8 min of illumination (Fig. 10a).

Note that already at a power density of 0.4 MW/cm$^2$ which is only slightly higher than that in the case of Fig. 10a, the evolution of the Raman spectra of heavily (10 at.%) zinc-doped $As_2Se_3$ film is quite monotonous: the broad "amorphous-like" maximum observed after 1 min illumination is within several minutes transformed into a considerably narrower asymmetric peak at 250 cm$^{-1}$ with a shoulder at the lower-frequency side.

One should emphasize as well that the photostructural changes observed in the Raman spectra of the zinc-doped $As_2Se_3$ films at sufficiently high laser power densities are irreversible, *i.e.* the corresponding features are retained in the spectra after the laser power density is reduced considerably below the threshold value.

## IV. DISCUSSION

Raman spectra of crystalline $As_2Se_3$ with an extensive series of narrow phonon peaks[40] are drastically different from the broad Raman maximum known for amorphous $As_2Se_3$ (Refs. 4, 33, 41, 42 and references therein) and observed in Fig. 5. The Raman evidence for the amorphous structure of the thermally evaporated Zn-doped $As_2Se_3$ films is undoubtable. Similar Raman-based conclusions were made earlier about the amorphous character of $As_2Se_3$ thin films prepared by pulsed laser deposition[34,41] and spin coating.[42] Meanwhile, for the thermally evaporated $As_2Se_3$ thin films the authors of Refs. 34 and 41 reported more complex Raman spectra with several pronounced narrower peaks in the range 200–250 cm$^{-1}$. This can be explained by the fact that fresh films obtained by those authors were structurally non-equilibrium with the presence of $Se_8$ rings, $Se_n$ chains as well as $As_4Se_3$ molecular structures, the narrower features of which in the Raman spectra vanished only after annealing for 1 h at 160–180°C or exposure to above-bandgap light.[34,41] The present data show that, contrary to the earlier studies,[34,41] our thermally evaporated films reveal amorphous structure. Most likely, this is related to the fact that room-temperature storage for about two months which elapsed from the preparation to the measurement, resulted in a relaxation to a more stable state with a structure close to that of the bulk glass. Such relaxation of the arsenic chalcogenide film structure under a room-temperature storage was reported earlier from optical studies.[43,44]

It is also important to note that the Raman measurements performed for the different spots across the sample area showed a very good reproducibility. This can be treated as evidence for a rather uniform dopant distribution across the film surface. Besides, the results obtained for the samples with similar compositions from the two batches prepared by two different approaches appeared quite

similar. This also correlates with the EDX data showing a good agreement of the results for samples with similar nominal Zn content originating from different batches. Note that the aforementioned gradient of the Zn content decreasing into the film depth revealed in the EDX and XPS data (Figs. 2 and 4, respectively) is noticeably similar to the cadmium concentration profile in $As_2Se_3$:Cd films reported in our recent study.[45]

The Raman data clearly demonstrate that rather weakly ($x \leq 5$ at.%) Zn-doped $As_2Se_3$ films, similarly to the undoped one, retain their amorphous structure under the laser beam illumination at the conditions specified above. However, more heavily ($x \geq 7$ at.%) Zn-doped $As_2Se_3$ films reveal clear photostructural changes when a certain threshold laser power density (its value depends on the zinc concentration and the laser wavelength) is achieved. This difference between the weakly and heavily Zn-doped films correlates as well with the AFM data showing much higher roughness for the more heavily doped films.

It is worth mentioning that the broad Raman maximum characteristic for amorphous $As_2Se_3$ is known to be an overlap of different vibrational maxima corresponding to various structural units, the vibrations of which are known to appear within the same frequency range, in particular, due to the small difference in the As and Se atomic masses.[33] In particular, the band at 227 $cm^{-1}$ is related to the vibrations of $AsSe_3$ pyramidal units that appear in the structure of bulk glasses.[33,46] For crystalline $As_2Se_3$, the most intense Raman peaks are also reported in this spectral range – 202, 216, 231, and 248 $cm^{-1}$.[40,47] Based on the studies of bulk glasses of the As–Se system, it was supposed that an excess of selenium can result in a noticeable contribution of –Se–Se–Se– chain vibrations with a maximum at 238 $cm^{-1}$.[33,42] However, a detailed study of Raman scattering in amorphous selenium suggests that intrachain bond-stretching vibrations of disordered selenium chains are responsible for the most intense band of amorphous Se at 250 $cm^{-1}$.[48] Vibrations of $Se_8$ rings can be revealed at high Se content at 252 $cm^{-1}$[33,42] or, based on the data for amorphous Se, near 260 $cm^{-1}$.[48] On the contrary, selenium deficiency results in an appearance of cage-like structural $As_4Se_4$ and $As_4Se_3$ units with characteristic vibration frequencies near 205 $cm^{-1}$ and 237 $cm^{-1}$, respectively.[33,46,49,50] A noticeable content of a dopant, especially if it is not a group III or group V element, can possibly result in a rearrangement of bonding configuration in the amorphous film and formation of the above mentioned structures depending on which of the two elements forming the film structural network (As or Se) remains in an excess while the other is preferably involved in binding with the dopant. As all the vibration frequencies for the above structural groups lie within a narrow range between 200 and 270 $cm^{-1}$, in the case of doping with zinc the situation becomes even more entangled since, as follows from the data for ZnSe[51–53] and $ZnAs_2$[54,55] crystals, the frequencies of vibrations of Zn–Se (205 and 252 $cm^{-1}$) and Zn–As bonds (the most intense features within 210–275 $cm^{-1}$) fall in the same spectral range. Therefore, the new features appearing in the rather heavily Zn-doped $As_2Se_3$ films under illumination by sufficiently intense laser light can be generally related to a variety of possible photostructural changes.

Evidently, simple partial substitution of amorphous $As_2Se_3$ film network atoms by Zn does not affect the Raman spectra which is clearly seen from Figs. 5 and 6. Only for heavily ($x \geq 7$ at.%) doped $As_2Se_3$:Zn films and only at laser power densities exceeding some threshold value (the latter depends on the Zn content and the laser wavelength) one can observe appearance and evolution of two narrower peaks at the low-frequency side (192–195 $cm^{-1}$) and the high-frequency side (241–250 $cm^{-1}$) of the broad initial band. Note that first we discuss the two above features in the qualitative sense regardless of the variation of their frequency positions with $x$ and $P_{exc}$. The quantitative aspect will be discussed below.

In our opinion, one may relate the emerging features to one of the two possible factors: (1) vibrations of zinc-containing structures (most likely nanoscale) being formed in the $As_2Se_3$ film due to the illumination, or (2) vibrations of the above discussed structures characteristic for the As-deficient (–Se–Se–Se– chains or, less likely, $Se_8$ rings) or Se-deficient ($As_4Se_4$ or $As_4Se_3$ cages) amorphous films which can emerge due to the partial substitution of atoms of the glass structural network by Zn atoms with a different electronic structure and a corresponding rearrangement of the glass structure. The probability of these two factors will be evaluated based on our experimental results and their comparison with other researchers' data.

As the structure of chalcogenide glasses is commonly described as a network of covalent bonds obeying the known 8–*N* rule,[46] the Zn dopant atoms are much more likely to substitute arsenic than selenium in the glass network. Therefore, the probability for structures typical for the Se-deficient amorphous films ($As_4Se_4$ or $As_4Se_3$ cages) is much higher than for the selenium chains or rings typical for the As-deficient material. Note that, as follows from the Raman study of $As_xSe_{100-x}$ glasses,[46] even a slight reduction of the Se content down from the 2:3 ratio results in a noticeable fraction of As-rich molecular units. Hence, the band at 241–250 $cm^{-1}$ is unlikely to be related to Se unit vibrations.

In a similar way, if one considers the possibility of photoinduced phase segregation, the formation of ZnSe crystallites seems to be much more probable than that of $ZnAs_2$ nanostructures. The formation of a noticeable amount of ZnSe crystallites then results in a selenium deficiency in the film structure and its rearrangement with a more noticeable fraction of the $As_4Se_4$ and $As_4Se_3$ cages. The question is whether the emerging Raman feature near 191–205 $cm^{-1}$ originates mostly from the vibrations of the $As_4Se_4$ cages or is it due to TO phonons of the ZnSe crystallites formed in the film. Likewise, what is responsible for the photoinduced Raman maximum appearing at 242–250 $cm^{-1}$: $As_4Se_3$ cage vibrations or ZnSe crystallite LO phonons?

Unfortunately, we have found no references in the literature with regard to Raman studies of Zn-doped $As_2Se_3$ films. Only a very limited number of studies was devoted to the Raman spectra of $As_2Se_3$ glasses and amorphous thin films doped with other metals.[56–59] For Ag-doped ones which are the most extensively studied, the initial broad band remains almost unchanged with the maximum near 225–235 $cm^{-1}$ at silver content below 5–12 at.% (depending on the film preparation method)[56–58] and shifts to 250 $cm^{-1}$ when it reaches 15 at.%.[57,58] The Raman spectra of bulk $As_2Se_3$ glasses retain the initial broad maximum centered at 227 $cm^{-1}$ with a shoulder near 250 $cm^{-1}$ under doping with Bi, Ge, Cd, Ag, Dy, Sm, Mn, and Sn, even though only for the latter the dopant concentration was up to 7.5 at.% while the content of other dopants did not exceed 1 at.%.[59]

Our measurements performed at similar conditions for thin $As_2Se_3$ films doped with Al (up to 7 at.%), Ga (up to 3 at.%), and

Si (up to 5 at.%) did not reveal any doping-induced or photoinduced changes in the Raman spectra either. For Cd-doped $As_2Se_3$ films (7–10 at.% Cd) we observed an additional relatively narrow peak near 208 $cm^{-1}$ on the background of the broad peak near 225 $cm^{-1}$, but no photoinduced changes resulting in any peak near 240–250 $cm^{-1}$ were detected.[45]

Among the variety of dopants in $As_2Se_3$ bulk glasses and amorphous films measured in the above mentioned studies by ourselves as well as other authors[56–59] there were group II, III, and IV elements as well as transition metals with different electronic structure which could possibly result in a rearrangement of the amorphous network with a noticeable content of units typical for the Se-deficient or As-deficient structures. However, a clear dopant-related peak in the range 240–250 $cm^{-1}$ was revealed only for Zn-doped films at sufficiently high laser power densities. Therefore, it seems unlikely that this intense peak can be related to $As_4Se_3$ cage vibrations of the Se-deficient amorphous structure which are known to be revealed at 238 $cm^{-1}$. An additional argument for this is provided by the data in Fig. 7b where one can clearly see that, in spite of the clearly visible transformation of the Raman spectra with time under the laser illumination (Fig. 7a), the position and the halfwidth of the amorphous $As_2Se_3$ maximum remain unchanged, only an additional Raman peak at about 250 $cm^{-1}$ appears, increasing only in intensity with again constant frequency and halfwidth. In our opinion, in the case of a rearrangement of structural units in the glass network, the evolution of the Raman spectra would be definitely much more complicated and could not be described by a simple appearance of a single new peak with basically the same frequency and halfwidth. We thus consider it reasonable to ascribe this relatively sharp feature with a maximum frequency position varying between 242 and 252 $cm^{-1}$ to the LO vibrations of ZnSe nanocrystallites which are formed in the heavily Zn-doped $As_2Se_3$ amorphous films under laser illumination exceeding certain power density threshold values.

In a similar way, the peak emerging at 191–205 $cm^{-1}$ in the heavily Zn-doped $As_2Se_3$ film spectra with increasing $P_{exc}$ can be ascribed to TO phonons of ZnSe crystallites rather than to the vibrations of $As_4Se_4$ cages in the glass network. Note that, as a rule, in II–VI nanocrystals Raman signal from resonance enhanced LO phonons strongly exceeds that from TO phonons (which are in general quite seldom observed) [Ref. 60 and references therein]. However, in our case, similarly to earlier studies of ZnSe nanocrystals[61] and nanoribbons,[53] we clearly observe a distinct TO phonon maximum near 200 $cm^{-1}$.

In our recent study for $As_2Se_3$ films doped with basically similar amounts of Cd, the electronic structure of which is very much similar to zinc, we also observed laser power-dependent appearance of new peaks in the Raman spectra at the positions close to the CdSe LO and 2LO phonon frequencies and related them to the laser-induced formation of CdSe nanocrystallites.[45] Similarly, distinct CdS LO and 2LO phonon peaks were observed for Cd-doped $As_2Se_3$ films at sufficiently high laser power density.[62]

ZnSe crystallites can be formed in laser-illuminated area of the Zn-doped film due to the intense diffusion of Zn atoms which is facilitated both thermally, due to the laser-induced heating of the illuminated area, and non-thermally, due to a dramatically increasing photoplasticity of the $As_2Se_3$ film. Note that the purely thermal contribution is definitely insufficient for the ZnSe nanocrystallite formation since we did not observe any similar effects in the Raman spectra of Zn-doped $As_2Se_3$ film samples annealed at 160 °C for 1 h.

Formation of II–VI nanocrystals at certain temperature conditions is well known for semiconductor-doped silicate glasses[63–65] where their presence can be clearly revealed from optical absorption as well as Raman spectra. Here one should take into account the features, specific for Raman scattering in nanocrystals, which can affect the position and shape of the observed peaks [Ref. 60 and references therein]. This is also essential in our case.

Namely, phonon confinement in nanocrystals due to their small size results in a relaxation of the selection rules enabling nonzero-wavevector phonons to contribute to the Raman spectrum which, as a rule, results in an asymmetric shape of the phonon peaks and even in their slight downward shift.[60,66–68] Besides, with increasing surface-to-volume ratio in nanocrystals, the contribution of surface phonons below the LO phonon frequency can become noticeable, leading as well to the LO phonon band asymmetry at the low-frequency side and a possible downward shift of its maximum.[67–69] Finally, phonon peaks in the Raman spectra of nanocrystals can shift upward or downward depending on the compressive or tensile stress which can exist in matrix-embedded nanocrystals.[60,70–73]

To estimate the confinement-related shift of the LO phonon peak in ZnSe nanocrystals, we apply the well-known Campbell-Fauchet approach,[66] according to which the first-order Raman spectrum $I(\omega)$ in a ZnSe quantum dot is given by

$$I(\omega) = A \int \frac{d^3q|C(0,\vec{q})|^2}{[\omega - \omega_{LO}(\vec{q})]^2 + (\Gamma_0/2)^2} \quad (1)$$

where $A$ is a coefficient, $\omega_{LO}(\vec{q})$ is the LO phonon dispersion curve, $\Gamma_0$ is the line width (FWHM in the bulk crystal), $C(0,\vec{q})$ is the Fourier coefficient of the phonon confinement function $W(\vec{r},L)$, $L$ being the nanocrystal diameter and $\vec{r}$ – radius-vector. The integration in Eq. (1) is performed over the entire Brillouin zone. The choice of the appropriate confinement function depends on the nanocrystal geometry and for spherical crystallite shape was optimized as[66]

$$W(\vec{r},L) = \exp(-8\pi^2 r^2/L^2), \quad (2)$$

with the corresponding Fourier coefficient

$$C(0,\vec{q}) \cong \exp(-q^2L^2/16\pi^2). \quad (3)$$

The LO phonon dispersion, similarly to Refs. 67 and 68, was taken as

$$\omega_{LO}(\vec{q}) = \omega_{LO}(\Gamma) - \Delta\omega_{LO}\sin^2(q/4) \quad (4)$$

where $\omega_{LO}(\Gamma)$ is the LO phonon frequency in the Brillouin zone center. The width $\Delta\omega_{LO}$ of the LO phonon branch in ZnSe is about 40 $cm^{-1}$.[74] The LO phonon line width $\Gamma_0$ for bulk single-crystal ZnSe is known to be 6 $cm^{-1}$ [75] The account of confinement-related $q\neq0$ phonons in the Raman spectra of ZnSe nanocrystals was calculated, following Eqs. (1), (3), (4). As follows from the calculations, the confinement-related downward shift of the LO phonon maximum is about 0.3 $cm^{-1}$ for the ZnSe nanocrystal diameter $L$=4 nm, 0.9 $cm^{-1}$ for $L$=2 nm, and 1.9 $cm^{-1}$ for $L$=1 nm which is already a double size of the unit cell.

Meanwhile, in our case the position of the Raman maximum which we ascribe to ZnSe crystallite LO phonon varies, depending on the Zn content, laser power density and illumination time, from 242 to 250 $cm^{-1}$. As follows from the calculations, such a strong downward shift by up to 10 $cm^{-1}$ from the LO phonon frequency (252 $cm^{-1}$) cannot be related to phonon confinement alone even for extremely small nanocrystals. Neither can this LO phonon peak shift be due to the surface phonon contribution since in this case the maximum position shift should be accompanied by a rather dramatic lineshape variation contrary to what is observed *e.g.* in Fig. 8c. Moreover, both the nonzero-wavevector and the surface phonon contributions, which could possibly cause a slight downward shift of the Raman peaks, should be more pronounced for smaller nanocrystals and diminish for the larger ones formed at higher laser power density and energy. Meanwhile, experimentally we observe that the ZnSe nanocrystal phonon frequencies are lower for the higher laser power densities and energies (when one should expect larger nanocrystals to be formed).

In our opinion, the observed broad variation of the LO and TO frequencies of ZnSe crystallites formed in the $As_2Se_3$ film under laser irradiation and depending on laser power density, energy and illumination time, should be related to the photoplastic effect which occurs in the film during the Raman measurement time. As mentioned above, in amorphous arsenic chalcogenides a photoinduced transfer of material from the illuminated area was reported.[35–37,76] The mechanism of this drastical change of viscosity enabling the film material transfer is non-thermal and the preferable direction of the mass transfer depends on the light polarization.[17,76,77] The photoplastic effect (photoinduced mass transfer from the laser spot) in amorphous arsenic chalcogenides is known to be reduced with going to lower temperatures.[78] In our case, the formation of a pit in the laser spot on the $As_2Se_3$ film surface is clearly confirmed by an AFM image (Fig. 11) taken after illumination of the film surface for 10 s.

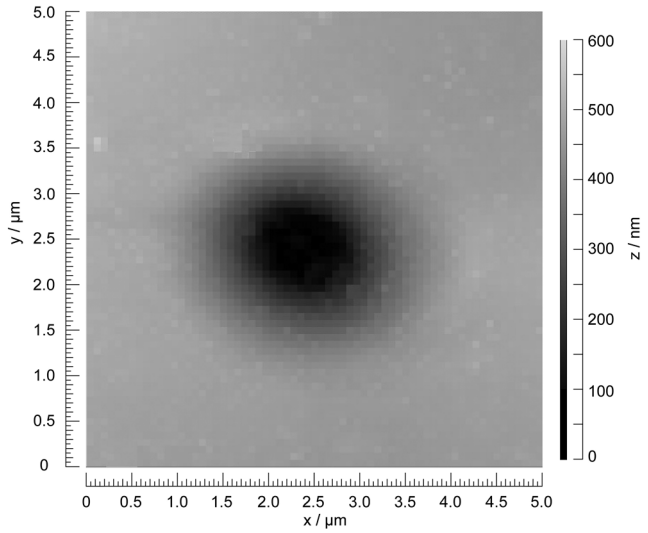


**FIG. 11**. AFM image of $As_2Se_3$ thin film after the illumination by 647.1 nm laser beam at the power density 0.3 $MW/cm^2$ for 10 s.

Since the material is partially removed from the spot area, a noticeable tensile strain emerges in the center of the pit. Therefore, the LO and TO phonon frequencies of the ZnSe crystallites observed in the spectra in Figs. 8–10 are noticeably lower than the values known for bulk crystal.

Assuming that the tensile strain is solely responsible for the shift, one can estimate the change in the ZnSe lattice parameter as[68]

$$\frac{\Delta a}{a} = \frac{(\omega_{NC}/\omega_{bulk})^{-1/\gamma} - 1}{3} \quad (5)$$

where $\omega_{bulk}$ and $\omega_{NC}$ are the LO phonon frequencies in the bulk and nanocrystalline crystals, $\gamma$ is the Grüneisen parameter (for ZnSe $\gamma$=0.85[79]). The maximal downward shift of the LO phonon frequency to 242 $cm^{-1}$ corresponds to the lattice parameter variation by 1.6 %.

The LO and TO phonon peak frequency shifts enable one to evaluate the stress value. From the studies of Raman scattering in ZnSe bulk crystals under pressure $p$, the following dependences of the LO and TO phonon frequencies were obtained:[79]

$$\omega_{LO} = 251.9 + 3.44p - 0.02p^2 \ (\mathrm{cm}^{-1}), \quad (6)$$

$$\omega_{TO} = 204.2 + 4.98p - 0.07p^2 \ (\mathrm{cm}^{-1}) \quad (7)$$

where the pressure $p$ values are in GPa. Dependences with very much similar coefficients were obtained for the experimental studies of ZnSe nanoribbons.[53] Assuming that the pressure coefficients should be similar for compressive and tensile strain, the use of Eqs. (6) and (7) in our case is justified. However, one should change the sign of the second term in the equations to the opposite and neglect the third term due to its small contribution. Then the stress value obtained for the case of the maximal downshift of the ZnSe TO and LO phonon frequencies to 192 and 242 $cm^{-1}$, respectively (Fig. 10a), is near 2.8 GPa (obtained from the TO phonon shift) and 2.9 GPa (from the LO phonon shift), and the good correlation of the two values seems quite reasonable.

Hence, the photoplastic effect results in stress in the $As_2Se_3$ film up to about 2.8–2.9 GPa. However, the stress value varies with the zinc content, laser power density and wavelength as well the illumination time and the data obtained cannot provide a clear correlation between these parameters and the stress value. Evidently, this requires a more detailed and targeted study.

The unusual non-monotonous behavior of the Raman spectra of the 10 at.% Zn-doped $As_2Se_3$ film at $P_{exc}$ = 0.3 $MW/cm^2$ (647.1 nm) observed in (Fig. 10a) gives a clear evidence how the photoplastic effect interferes with the Raman measurement. The bands which emerge at 192 and 242 $cm^{-1}$ during the second minute of illumination, basically similar to those observed for the less-heavily doped $As_2Se_3$:Zn films at sufficiently high power densities (Figs. 7–9), indicate the formation of ZnSe crystallites under rather strong tensile strain. However, due to the photoplastic effect the film material exposed to the illumination (together with the nanocrystals) is radially removed from the laser spot, where a pit is formed on the film surface. The exciting laser beam in the depth of the pit becomes slightly defocused and the Zn content at this depth is lower, hence the power density is no longer sufficient to induce the ZnSe nanocrystal formation in the film. Therefore, the Raman spectra taken thereafter provide evidence for the amorphous film

structure retained. This may result in a misleading conclusion of reversible photostructural changes in $As_2Se_3$:Zn films similar to those observed in an early Raman study.[15] However, this only means that the ZnSe nanocrystals are transferred from the laser beam probing area together with the surrounding film material, but do not dissolve back in the amorphous film network.

At a slightly higher power density of 0.4 MW/cm$^2$ (Fig. 10b) the LO phonon peak of the ZnSe crystallites at 250 cm$^{-1}$ is clearly observed without any sign of vanishing. Evidently, this laser power density is sufficient to enable the photoinduced changes in the film structure even by a somewhat defocused beam in the depth of the pit.

In some cases at sufficiently high power densities we observed the peak near 250 cm$^{-1}$ which we claim to originate from the LO phonons of ZnSe crystallites being formed, but did not observe a clear TO phonon band near 200 cm$^{-1}$ (See e. g. Fig. 10). One should note that the situation when only LO phonon bands are observed in the Raman spectra, is rather typical for matrix-embedded nanocrystals[60,67–71] when, due to the small fraction of the nanocrystals in the sample scattering volume, resonance Raman scattering conditions are required to provide a detectable Raman signal and the resonance enhancement is much stronger for the LO phonons.

## V. CONCLUSIONS

Zn-doped $As_2Se_3$ films with nominal zinc content $x$ up to 10 at.% were prepared by thermal evaporation. Their structure was confirmed to be amorphous by Raman scattering data. The AFM studies showed undoped and rather weakly Zn-doped ($x \leq 5$ at.%) $As_2Se_3$ films to be much smoother (with a surface roughness $R_a$ of 1.1–3.3 nm) than the films with higher Zn content, for which $R_a$ ranges from 17 to 44 nm.

EDX studies performed at different exciting electron energies (5–30 keV) showed a strong gradient of the Zn content decreasing into the film depth. The decrease of the zinc concentration in the films with depth is confirmed by the element content profiles built on the base of XPS data measured for the Zn-doped $As_2Se_3$ films after sequential sessions of $Ar^+$ ion sputtering. Meanwhile, a qualitative correlation is observed between the nominal $x$ values and the content of zinc in the surface area determined from the EDX and XPS data.

While the weakly doped $As_2Se_3$:Zn ($x \leq 5$ at.%) films retain their amorphous structure in the whole range of the laser power densities $P_{exc}$ used for the Raman excitation, the heavily Zn-doped ($x \geq 7$ at.%) $As_2Se_3$ films reveal changes in the spectra in the course of the Raman measurement in case that $P_{exc}$ exceeds a certain threshold value depending on the zinc content and the laser wavelength. These changes are observed as new peaks near 191–205 cm$^{-1}$ and 242–250 cm$^{-1}$ which appear in the Raman spectra after a certain illumination time. The analysis revealed that the maxima can hardly be explained by the photostructural changes in the amorphous film with the formation of units characteristic for As-deficient (selenium chains or rings) or Se-deficient ($As_4Se_4$ or $As_4Se_3$ cages) structures. The new Raman features are attributed to the TO and LO vibrations of ZnSe nanocrystallites formed in the film under the illumination. The variation of the ZnSe crystallite TO and LO phonon frequencies with the illumination duration and the laser power density is explained by the tensile strain on the ZnSe crystallites due to the simultaneous photoplastic effect (partial removal of the material from the laser spot) of non-thermal origin observed in the $As_2Se_3$ films. The tensile strain value, estimated from the TO and LO phonon frequency shift, is shown to vary up to 2.9 GPa depending on the laser power density and wavelength as well as on the illumination time.

## ACKNOWLEDGMENTS

Yu. Azhniuk and E. Sheremet are grateful to DFG Research Unit SMINT (FOR 1713) for the financial support. Yu. Azhniuk is grateful to DAAD (Funding programme ID 57313677, Personal ref. No. 91574393) for the scholarship supporting his research stay at Chemnitz University of Technology. E. Sheremet thanks Tomsk Polytechnic University Competitiveness Enhancement Program.

## REFERENCES

[1] A. V. Kolobov and K. Tanaka, "Photoinduced phenomena in amorphous chalcogenides: From phenomenology to nanoscale," in *Handbook of Advanced Electronic and Photonic Materials and Devices*, edited by H. S. Nalwa (Academic Press, San Diego, 2001), Vol. 5, pp. 47–85.
[2] M. Frumar, B. Frumarová, T. Wágner, and P. Němec, "Photo-induced phenomena in amorphous and glassy chalcogenides," in: *Photo-Induced Metastability in Amorphous Semiconductors*, edited by A. V. Kolobov (Wiley-VCH, Weinheim, 2003), pp. 23–44.
[3] F. Wang and P. Boolchand, "Photostructural transformations and global connectedness of network glasses," in: *Non-Crystalline Materials for Optoelectronics*, edited by G. Lucovsky and M. Popescu (INOE, Bucharest, 2004), pp. 15–41.
[4] A. V. Kolobov and J. Tominaga, *Metastability and Phase Change Phenomena* (Springer, Berlin, 2012).
[5] Ke. Tanaka and K. Shimakawa, *Amorphous Chalcogenide Semiconductors and Related Materials* (Springer, Berlin, 2011).
[6] T. Ohta and S. R. Ovshinsky, "Phase-change optical storage media," in: *Photo-Induced Metastability in Amorphous Semiconductors*, edited by A. V. Kolobov (Wiley-VCH, Weinheim, 2003), pp. 310–326.
[7] A. Zakery and S. R. Elliott, J. Non-Cryst. Solids **330**, 1 (2003).
[8] Q. Coulombier, L. Brilland, P. Houizot, T. Chartier, T. N. N'Guyen, F. Smektala, G. Renversez, A. Monteville, D. Méchin, T. Pain, H. Orain, J.-C. Sangleboeuf, and J. Trolès, Opt. Express **18**, 9107 (2010).
[9] C. Florea, J. S. Sanghera, L. B. Shaw, V. Q. Nguyen, and I. D. Aggarwal, Mater. Lett. **61**, 1271 (2007).
[10] N. Hô, M. C. Phillips, H. Qiao, P. J. Allen, K. Krishnaswami, B. J. Riley, T. L. Myers, and N. C. Anheier, Jr., Opt. Lett. **31**, 1860 (2006).
[11] S. O. Kasap and J. A. Rowlands, in: *Insulating and Semiconducting Glasses*, edited by P. Boolchand (World Scientific, Singapore, 2000), pp. 781–811.
[12] A. Kovalskiy, M. Vlcek, K. Palka, J. Buzek, J. York-Winegar, J. Oelgoetz, R. Golovchak, O. Shpotyuk, and H. Jain, Appl. Surf. Sci. **394**, 604 (2017).
[13] M. Malyovanik, S. Ivan, A. Csik, G. A. Langer, D. L. Beke, and S. Kökényesi, J. Appl. Phys. **93**, 139 (2003).
[14] R. Golovchak, A. Kovalskiy, A. C. Miller, H. Jain, and O. Shpotyuk, Phys. Rev. B **76**, 125208 (2007).
[15] L. Abdulhalim and R. Beserman, Solid State Commun. **64**, 951 (1987).
[16] A. Kolobov, H. Oyanagi, A. Roy, and K. Tanaka, J. Non-Cryst. Solids **277-230**, 710 (1998).
[17] S. N. Yannopoulos, "Photo-plastic effects in chalcogenide glasses: Raman scattering studies," in: *Photo-Induced Metastability in Amorphous Semiconductors*, edited by A. V. Kolobov (Wiley-VCH, Weinheim, 2003), pp. 119–137.
[18] S. N. Yannopoulos, K. S. Andrikopoulos, D. Th. Kastrissios, and G. N. Papatheodorou, Phys. Status Solidi B **249**, 2005 (2012).
[19] K. Ramesh, N. Ramesh Rao, K. S. Sangunni, and E. S. R. Gopal, Phys. Status Solidi **235**, 536 (2003).
[20] K. Ogusu and K. Shinkawa, Opt. Express **17**, 8165 (2009).

[21] Yu. M. Azhniuk, A. V. Gomonnai, V. M. Rubish, M. Yu. Rigan, A. M. Solomon, O. O. Gomonnai, O. G. Guranich, I. Petryshynets, and D. R. T. Zahn, J. Phys. Chem. Solids **74**, 1452 (2013).
[22] Yu. M. Azhniuk, P. Bhandiwad, V. M. Rubish, P. P. Guranich, O. G. Guranich, A. V. Gomonnai, and D. R. T. Zahn, Ferroelectrics **416**, 113 (2011).
[23] Yu. M. Azhniuk, V. Stoyka, I. Petryshynets, V. M. Rubish, O. G. Guranich, A. V. Gomonnai, and D. R. T. Zahn, Mater. Res. Bull. **47**, 1520 (2012).
[24] V. Benekou, L. Strizik, T. Wagner, S. N. Yannopoulos, A. Lindsay Greer, and J. Orava, J. Appl. Phys. **122**, 173101 (2017).
[25] J. George, *Preparation of Thin Films* (Marcel Dekker Inc., New York, 1992), pp. 6–13.
[26] A. V. Naumkin, A. Kraut-Vass, S. W. Gaarenstroom, and C. J. Powell, "NIST x-ray photoelectron spectroscopy database," NIST, Stand. Ref. Database 20, Version 4.1 (2012).
[27] O. Kondrat, R. Holomb, N. Popovich, V. Mitsa, M. Veres, A. Csik, N. Tsud, V. Matolín, and K. C. Prince, J. Non. Cryst. Solids **410**, 180 (2015).
[28] M. Shenasa, S. Sainkar, and D. Lichtman, J. Electron Spectrosc. Related Phenomena **40**, 329 (1986).
[29] G. De Moor, A. Ozer, and I. Heyse, J. Non. Cryst. Solids **18**, 197 (1975).
[30] T. Ueno and A. Odajima, Jpn. J. Appl. Phys. **21**, 230 (1982).
[31] K. Antoine, J. Li, D. A. Drabold, H. Jain, M. Vlček, and A. C. Miller, J. Non. Cryst. Solids. **326-327**, 248 (2003).
[32] R. Golovchak, O. Shpotyuk, A. Kovalskiy, A. C. Miller, J. Čech, and H. Jain, Phys. Rev. B **77**, 172201 (2008).
[33] V. Kovanda, M. Vlček, and H. Jain, J. Non-Cryst. Solids **326-327**, 88 (2003).
[34] M. Frumar, B. Frumarova, P. Nemec, T. Wagner, J. Jedelsky, and M. Hrdlicka, J. Non-Cryst. Solids **352**, 544 (2006).
[35] M. L. Trunov, S. N. Dub, P. M. Nagy, and S. Kokenyesi, J. Phys. Chem. Solids **68**, 1062 (2007).
[36] S. N. Yannopoulos and M. L. Trunov, Phys. Status Solidi B. **246**, 1773 (2009).
[37] M. L. Trunov, P. M. Lytvyn, P. M. Nagy, and O. M. Dyachyns'ka, Appl. Phys. Lett. **96**, 111908 (2010).
[38] J.-L. Adam and X. Zhang, *Chalcogenide Glasses: Preparation, Properties and Applications* (Woodhead Publishing, Cambridge, Philadelphia, New Delhi, 2014), p. 12.
[39] G. A. N. Connell, "Optical properties of amorphous semiconductors," in: *Amorphous Semiconductors*, ed. by M. Brodsky (Springer, Berlin, 1985), pp. 73–111.
[40] R. Zallen, M. L. Slade, and A. T. Ward, Phys. Rev. B **3**, 4257 (1971).
[41] P. Němec, J. Jedelský, M. Frumar, M. Štábl, and M. Vlček, J. Phys. Chem. Solids **65**, 1253 (2004).
[42] Y. Zou, H. Lin, O. Ogbuu, L. Li, S. Danto, S. Novak, J. Novak, J. D. Musgraves, K. Richardson, and J. Hu, Opt. Mater. Express **2**, 1723 (2012).
[43] V. M. Kryshenik and V. I. Mikla, Mater. Sci. Eng. B **100**, 292 (2003).
[44] V. M. Kryshenik, V. P. Ivanitsky, and V. S. Kovtunenko, J. Optoelectron. Adv. Mater. **7**, 2953 (2005).
[45] Yu. M. Azhniuk, D. Solonenko, E. Sheremet, V. Yu. Loya, I. V. Grytsyshche, S. Schulze, M. Hietschold, A. V. Gomonnai, and D. R. T. Zahn, Thin Solid Films **651**, 163 (2018).
[46] G. Yang, B. Bureau, T. Rouxel, Y. Gueguen, O. Gulbiten, C. Roiland, E. Soignard, J. L. Yarger, J. Troles, J.-C. Sangleboeuf, and P. Lucas, Phys. Rev. B **82**, 195206 (2010).
[47] E. Finkman, A. P. DeFonzo, and J. Tauc, In: *Proceedings of the 12th International Conference on the Physics of Semiconductors* (Springer, Wiesbaden, 1974), vol. 1, pp. 1022–1026.
[48] S. N. Yannopoulos and K. S. Andrikopoulos, J. Chem. Phys. **121**, 4747 (2004).
[49] P. Němec, J. Jedelský, M. Frumar, M. Štábl, and Z. Černošek, Thin Solid Films **484**, 140 (2005).
[50] P. Němec and M. Frumar, Thin Solid Films **516**, 8377 (2008).
[51] U. Rössler, in: *Landolt-Börnstein - Group III "Condensed Matter"*, Volume 44 "Semiconductors", Subvolume F "New Data and Updates for several Semiconductors with Chalcopyrite Structure, for several II-VI Compounds and diluted magnetic IV-VI Compounds" (Springer, Berlin, 2013), pp. 240–245.
[52] D. Nesheva, M. J. Šćepanović, S. Aškrabić, Z. Levi, I. Bineva, and Z. V. Popović, Acta Physica Polonica A **116**, 75 (2009).
[53] L. D. Yao, F. F. Wang, X. Shen, S. J. You, L. X. Yang, S. Jiang, Y. C. Li, K. Zhu, Y. L. Liu, A. L. Pan, B. S. Zou, J. Liu, C. Q. Jin, and R. C. Yu, J. Alloys Compounds **480**, 798 (2009).
[54] J. Weszka, M. Balkanski, M. Jouanne, D. I. Pishchikov, and S. F. Marenkin, Phys. Status Solidi B **171**, 275 (1992).
[55] O. A. Yeshchenko, I. M. Dmitruk, S. V. Koryakov, M. P. Galak, I. P. Pundyk, and L. M. Hohlova, Physica B **368**, 8 (2005).
[56] A. V. Stronski, M. Vlček, A. I. Stetsun, A. Sklenař, and P. E. Shepeliavyi, Semicond. Phys., Quantum Electron. & Optoelectron. **2**(2), 63 (1999).
[57] K. Ogusu, T. Kumagai, Y. Fujimori, and M. Kitao, J. Non-Crystal. Solids **324**, 118 (2003).
[58] K. Ogusu, Sh. Maeda, M. Kitao, H. Li, and M. Minakata, J. Non-Crystal. Solids **347**, 159 (2004).
[59] M. Iovu, E. I. Kamitsos, C. P. E. Varsamis, P. Boolchand, and M. Popescu, J. Optoelectron. Adv. Mater. **7**, 1217 (2005).
[60] V. M. Dzhagan, Yu. M. Azhniuk, A. G. Milekhin, and D. R. T. Zahn, J. Phys. D **51**, 503001 (2018).
[61] X. Fu, H. An, and W. Du, Mater. Lett. **59**, 1484 (2005).
[62] Yu. M. Azhniuk, V. M. Dzhagan, D. Solonenko, A. Mukherjee, V. Yu. Loya, I. V. Grytsyshche, V. V. Lopushansky, A. V. Gomonnai, and D. R. T. Zahn, Phys. Status Solidi B **256**, 1800298 (2019).
[63] N. F. Borrelli, D. Hall, H. Holland, and D. Smith, J. Appl. Phys. **61**, 5399 (1987).
[64] L.-C. Liu and S. H. Risbud, J. Appl. Phys. **68**, 28 (1990).
[65] U. Woggon, *Optical Properties of Semiconductor Quantum Dots* (Springer-Verlag, Berlin, 1997).
[66] P. M. Fauchet and I. H. Campbell, Critical Reviews in Solid State and Materials Sciences **14**, S79 (1988).
[67] A. Roy and A. K. Sood, Phys. Rev. B **53**, 12127 (1996).
[68] A. V. Gomonnai, Yu. M. Azhniuk, V. O. Yukhymchuk, M. Kranjčec, and V. V. Lopushansky, Phys. Status Solidi B **239**, 490 (2003).
[69] V. M. Dzhagan, M. Ya. Valakh, C. Himcinschi, A. G. Milekhin, D. Solonenko, N. A. Yeryukov, O. E. Raevskaya, O. L. Stroyuk, and D. R. T. Zahn, J. Phys. Chem. C **118**, 19492 (2014).
[70] G. Scamarcio, M. Lugar, and D. Manno, Phys. Rev. B **45**, 13792 (1992).
[71] Yu. M. Azhniuk, Yu. I. Hutych, V. V. Lopushansky, A. E. Raevskaya, A. L. Stroyuk, S. Ya. Kuchmii, A. V. Gomonnai, and D. R. T. Zahn, J. Phys.: Conf. Ser. **78**, 012017 (2007).
[72] V. M. Dzhagan, M. Ya. Valakh, A. G. Milekhin, D. R. T. Zahn, E. Cassette, C. Javaux, T. Pons, and B. Dubertret, J. Phys. Chem. C **117**, 18225 (2013).
[73] G. Zatryb, J. Misiewicz, P. R. J. Wilson, J. Wojcik, P. Mascher, and A. Podhorodecki, Thin Solid Films **571**, 18 (2014).
[74] B. Hennion, F. Moussa, G. Pepy, and K. Kunc, Phys. Lett. **36A**, 376 (1971).
[75] D. Nesheva, M. J. Šćepanović, S. Aškrabić, Z. Levi, I. Bineva, and Z. V. Popović, Acta Phys. Polon. A **116**, 75 (2009).
[76] J. Teteris, U. Gertners, and M. Reinfelde, Phys. Status Solidi C **8**, 2780 (2011).
[77] V. M. Kryshenik, M. L. Trunov, and V. P. Ivanitsky, J. Optoelectron. Adv. Mater. **9**, 1949 (2007).
[78] M. L. Trunov and P. M. Lytvyn, J. Non-Cryst. Solids **493**, 86 (2018).
[79] C.-M. Lin, D.-S. Chuu, T.-J. Yang, W.-C. Chou, J. Xu, and E. Huang, Phys. Rev. B **55**, 13641 (1997).